CHEMISTRY OF MATERIALS

ARTICLE

pubs.acs.org/cm

# Interplay of Magnetism and Bonding in $GaV_{4-x}Cr_xSe_8$

Daniel Bichler and Dirk Johrendt*

Department Chemie, Ludwig-Maximilians-Universität München, Butenandtstrasse 5-13 (Haus D), 81377 München, Germany

Supporting Information

**ABSTRACT:** The solid solution $GaV_{4-x}Cr_xSe_8$ ($x$ = 0−4) was synthesized; their crystal structures and magnetic properties were determined and compared with results of ab initio density functional theory (DFT) calculations. The compounds crystallize in the $GaMo_4S_8$-type structure ($F\bar{4}3m$), consisting of $GaS_4$ tetrahedra and heterocubane-like $(V_{4-x}Cr_x)Se_4$ units. Significant metal−metal bonding within tetrahedral metal clusters exists up to $GaV_2Cr_2Se_8$ ($x$ = 2), while the bonds gradually disperse when $x$ > 2. The dissolving of the metal−metal bonds is associated with large increases in the magnetic moments. This can be explained by metal−metal bonded tetrahedral $V_{4-x}Cr_x$ clusters with (small) magnetic moments localized in cluster molecular orbitals for $x \leq 2$, whereas the magnetism of Cr-rich compounds is better described by a mixture of $V_2Cr_2$ clusters and nonbonded Cr atoms with stronger magnetism. $GaV_4Se_8$ and hypothetical $GaCr_4Se_8$ were investigated as model systems by ab initio DFT calculations. Thus, the ground state of $GaV_4Se_8$ contains $V_4$ cluster units with small magnetic moments, while $GaCr_4Se_8$ has no tendency to form strong Cr−Cr bonds, but a much higher magnetic moment, both in good agreement with the experimental data.

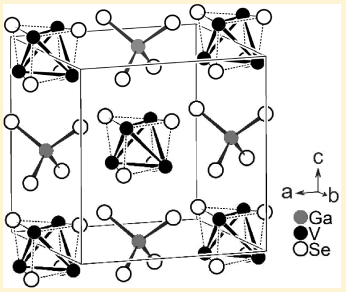


**KEYWORDS:** metal cluster, vanadium, chromium, magnetism, Mott insulators

## INTRODUCTION

Compounds with the $GaMo_4S_8$ structure type[1] represent a special type of Mott insulator in which electronic conduction takes place as electrons hop between widely separated $M_4$ clusters ($M$ = Ti, V, Nb, Ta, or Mo)[1−6] and not between single atoms as in classical Mott insulators like NiO. These materials exhibit an impressive variety of interesting properties, among them 4$d$ ferromagnetism,[5,7] phase transitions,[8,9] heavy fermion behavior,[10] superconductivity,[3,11] high magnetoresistance,[12] and electric pulse-induced resistivity switching.[13,14] One of the first thoroughly investigated compounds in this system is $GaV_4S_8$,[2,9,15−19] which consists of a rock salt-like assembly of $GaS_4^{5+}$ tetrahedra and cubane-like $V_4S_4^{5-}$ units with significant V−V bonding as shown in Figure 1. The structure can also be derived from the cubic spinel structure. In the $AB_2X_4$ spinel, the $A$ atoms order in one-eighth of the tetrahedral voids and the $B$ atoms in half of the octahedral voids of a cubic closed packing of $X$ atoms. In $GaMo_4S_8$, one-half of the tetrahedral $A$ sites remain empty, which causes a reduction in symmetry from $Fd\bar{3}m$ (spinel) to $F\bar{4}3m$ ($GaMo_4S_8$-type). The 8$a$ site (0,0,0) of the spinel splits into sites 4$a$ (0,0,0) and 4$c$ ($^1/_4$,$^1/_4$,$^1/_4$) in $F\bar{4}3m$, where only 4$a$ is occupied. The 16$d$ site ($^5/_8$,$^5/_8$,$^5/_8$) occupied by the $B$ atoms becomes the 16$e$ site ($x$,$x$,$x$) in $F\bar{4}3m$, which allows the $B$ atoms on this site to dislocate along the body diagonal of the unit cell. As a result, tetrahedral $M_4$ clusters emerge when the position of the $B$ atoms shifts from $x = {}^5/_8$ in the spinel type. The 32$e$ site of the $X$ atoms splits into two 16$e$ sites in $F\bar{4}3m$, allowing two different $X$ atom positions. The formation of $M_4$ clusters causes significant changes in the physical properties. The metal electrons not incorporated in $M$−S bonds localize in cluster molecular orbitals (Figure 2). Because the clusters are widely separated (>390 pm), orbitals of different clusters do not overlap and the compound becomes nonmetallic. Electric conduction takes place as the electrons hop between the clusters. As we reported earlier, fundamental physical properties such as electronic conduction and magnetism can be rationalized by a simple cluster molecular orbital scheme.[2,9,18,20,21] Six $M$−$M$ bonding orbitals are available for a maximum of 12 electrons. $GaV_4S_8$ contains seven electrons in the $V_4$ unit according to the ionic formula splitting $(Ga^{3+})(V^{3.25+})_4(S^{2-})_8$, while 11 electrons are present in the $Mo_4$ cluster of $GaMo_4S_8$. Figure 1 shows the cluster molecular orbitals. The highest occupied molecular orbital ($t_2$) is 3-fold degenerate and filled with one or five electrons in $GaV_4S_8$ or $GaMo_4S_8$, respectively. This results in one unpaired electron per cluster for both, in good agreement with experimental results. The model also holds for $GeV_4S_8$ with two unpaired electrons of eight that occupy the $V_4$ cluster orbital. All known compounds with $GaMo_4S_8$ structure show ferro- or antiferromagnetic ordering at low temperatures and are narrow gap semiconductors ($E_G$ < 0.2 eV). While the isotypic compounds $GaM_4Se_8$ exist with all group 5 metals ($M$ = V, Nb, or Ta), $GaMo_4Se_8$ is still the only group 6 metal representative, especially with $GaCr_4Se_8$ beings unknown. Recently, we reported the $Ga_xV_{4-y}Cr_yS_8$ series ($x$ = 1 or 1.33; $y$ = 0−4),[22] in which additional gallium atoms occupy the 4$c$ site at higher chromium concentrations.

In this paper, we report about the crystal structures and properties of the $GaV_{4-x}Cr_xSe_8$ series and compare the obtained results to ab initio density functional theory (DFT) calculations.

**Received:** March 17, 2011
**Revised:** April 28, 2011
**Published:** May 16, 2011





dx.doi.org/10.1021/cm200776v | *Chem. Mater.* 2011, 23, 3014–3019

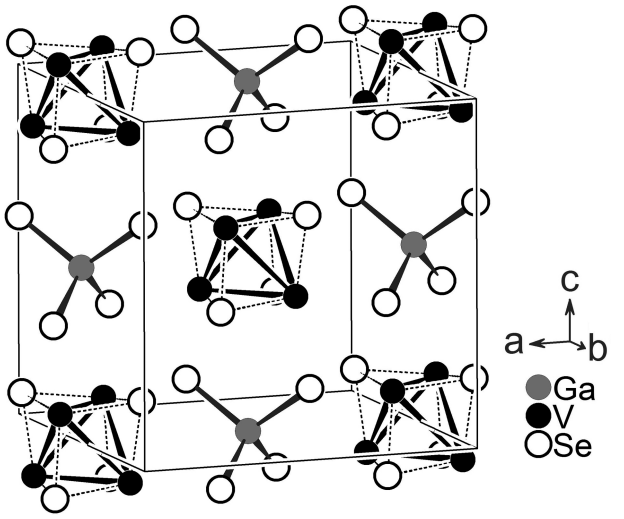


**Figure 1.** Crystal structure of $GaV_4Se_8$, depicted as $GaSe_4^{5-}$ tetrahedra and cubanelike $V_4Se_4^{5+}$ units in a NaCl-like assembly. The V−V bond lengths (black lines) are ∼290 pm.

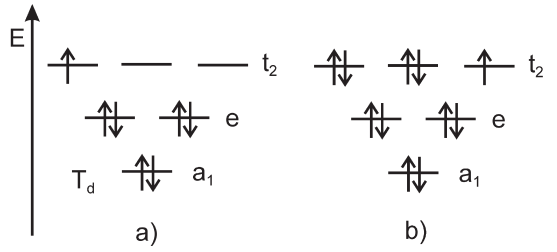


**Figure 2.** (a) Cluster molecular orbital scheme for $GaV_4Se_8$ occupied by 7 electrons. (b) Cluster molecular orbital scheme of $GaMo_4S_8$ and hypothetical $GaCr_4Se_8$ occupied by 11 electrons.

## EXPERIMENTAL SECTION

**Synthesis.** Starting materials were gallium ingots (99.999%, Alfa Aesar), vanadium granules (99.5%, Alfa Aesar), chromium powder (99.8%, Alfa Aesar), and selenium granules (99.999%, ChemPur). Powder samples of $GaV_{4-x}Cr_xSe_8$ ($x = 0-4$) were prepared by reacting stoichiometric mixtures of the elements in silica tubes under an argon atmosphere at 1023 K, heated at a rate of 50 K/h, and held at the final temperature for 12 h. After this initial heating, the samples were cooled to room temperature, ground, and repeatedly annealed at 1073 K between 15 and 50 h until homogeneous phases were obtained. To achieve this, some samples had to be annealed as many as 10 times. Cr-rich samples had to be synthesized with a slight excess of Se to prevent the formation of $Cr_2Se_3$ because of the evaporation of selenium from the reaction mixture. The excess of Se usually crystallized at the top of the silica tube.

**Energy Dispersive X-ray Measurements.** Semiquantitative compositions were obtained by energy dispersive X-ray (EDX) analysis using a scanning electron microscope (JEOL JSM-6500 FE-SEM) equipped with an EDX detector (Oxford Instruments). The samples were prepared on a brazen sample holder and by sputtering coated with carbon to ensure electric conductivity. Several points on the sample were investigated, and the results were averaged (standards being Ga/GaP, V/V, Cr/Cr, and Se/Se).

**X-ray Powder Diffraction.** X-ray powder patterns were recorded using a Stoe Stadi-P diffractometer [Cu $K\alpha_1$ radiation, Ge(111) monochromator, 7° position sensitive detector, Si as the external standard] or a Huber G670 imaging plate diffraction system [Cu $K\alpha_1$ radiation, Ge(111) monochromator, $SiO_2$ as the external standard]. Lattice parameters were refined using the Rietveld method.

**Single-Crystal X-ray Diffraction.** Crystals were selected from the polycrystalline samples, glued to thin silica fibers, and checked for their quality by Laue photographs. Suitable crystals were used to collect complete intensity data sets in the oscillation mode with a Stoe IPDS-1 imaging plate detector (Mo Kα radiation, graphite monochromator). Data processing and numerical absorption corrections were performed using X-RED.[23] The structures were determined with the direct methods program SHELXS and refined with full-matrix least-squares using SHELXL.[24] All final cycles included anisotropic displacement parameters. Because of the almost identical scattering powers of Cr and V, we were unable to refine the V:Cr ratios and have thus fixed them to the nominal composition (all in good agreement with the EDX measurements). However, certain deviations from the nominal compositions of approximately ±10% are possible.

**Electrical Resistivity.** Cold pressed powder pellets (diameter of 6 mm, height of ∼1 mm) of the samples were sintered at 873 K for 12 h. The pellets were contacted with silver wires and silver paste, and the specific electrical resistivity was measured between 8 and 300 K using a dc four-point current reversal method.[25]

**Magnetic Measurements.** The magnetic properties of the samples were measured utilizing a SQUID magnetometer (MPMS-XL Quantum Design Inc.). Fine ground powder samples were inserted in capsules and those into a straw with known diamagnetism. The magnetic susceptibilities of the samples were collected in a temperature range of 1.8−300 K with magnetic flux densities of ≤5 T. To determine Curie points of ferromagnetic samples, we took zero-field-cooled and field-cooled measurements at 3 mT. Neel temperatures for antiferromagnetic samples were set at the exact maximum of the bend in magnetic susceptibility and inverse magnetic susceptibilities. The data were corrected for diamagnetic contributions of the capsule, the straw, and the sample using diamagnetic increments.[26]

**DFT Calculations.** Quantum mechanical calculations were conducted with the Augmented Plane Wave Plus Local Orbitals Full Potential Program WIEN2k.[27] Input data for $GaV_4Se_8$ were taken from single-crystal X-ray measurements; input data for hypothetical $GaCr_4Se_8$ were taken from single-crystal X-ray data of $GaV_{0.5}Cr_{3.5}Se_8$. In both cases, the $x$ positions of the $M$ atoms at Wyckoff positon 16$e$ in $F\bar{4}3m$ were varied between 0.625 (spinel) and 0.597 (cluster). All other atomic positions were allowed to relax. For hypothetical $GaCr_4Se_8$, we conducted a second calculation with the magnetic moment fixed to one unpaired electron per formula to investigate the energy surface. All calculations used a grid of 4 × 4 × 4 irreducible $k$ points and a plane wave cutoff $R_{min}K_{max}$ of 7.0, resulting in approximately 2500 plane waves. The exchange correlation functional of Perdew, Burke, and Ernzerhof was used.[28]

## RESULTS

**Crystal Structures.** The X-ray powder patterns of all samples could be indexed with cubic face-centered unit cells, and lattice parameters were extracted from subsequent Rietveld refinements (Figure 3). The lattice parameters continuously increase with $x$ as shown in Figure 4.

Single-crystal data sets could be refined using cubic space group $F\bar{4}3m$. Atomic positions and important distances can be found in the Supporting Information. Further details of the crystal structure determinations (CIF data) are deposited and can be obtained from Fachinformationszentrum Karlsruhe (D-76344 Eggenstein-Leopoldshafen, Germany) (http://www.fiz-karlsruhe.de/icsd.html) by quoting registry numbers 420170−420176.

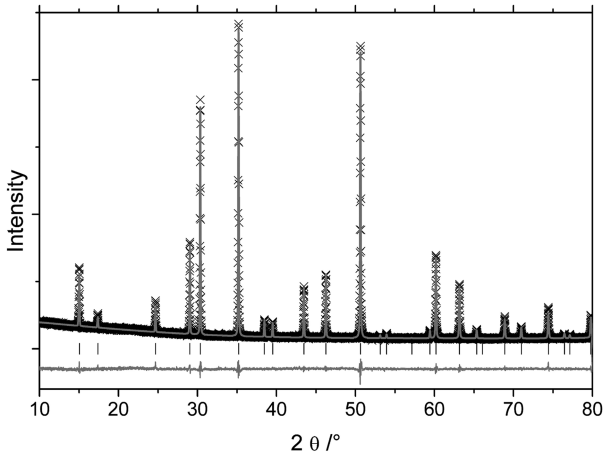


**Figure 3.** Rietveld fit of $GaV_2Cr_2Se_8$. Crosses mark the experimental pattern; the gray line overlaying the crosses is the simulated pattern, and the gray line below them is the difference curve. Tick marks denote reflection positions.

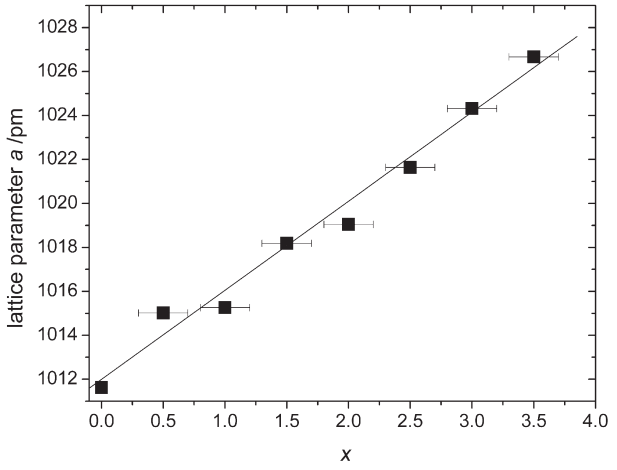


**Figure 4.** Lattice parameters of $GaV_{4-x}Cr_xSe_8$ from Rietveld refinements. The gray line is a guide to the eye. Errors in $x$ are estimated from EDX results. Errors in $a$ are smaller than the symbols.

As an important result and in contrast to $Ga_xV_{4-y}Cr_yS_8$,[22] no additional (gallium) atoms were detected in the empty tetrahedral holes at 4*c*. Atomic positions of the selenium that together with gallium form the $GaSe_4$ tetrahedra (Se2) hardly change throughout the series. On the other hand, the positions of Se1 and Cr/V that form the cubane-like $M_4Se_4$ unit change toward the spinel type when $x > 2$ (see Figure 5). As a result, on the V-rich side of the series, $M_4$ clusters with rather short $M-M$ distances are present. At the Cr-rich side, the $M-M$ distances grow to ~330 pm, which are too long to be considered bonds between the $M$ atoms (Figure 6). Here the description as a distorted defect spinel-type structure is much more suitable than the description as a cluster compound with $GaMo_4S_8$-type structure. Thus, we observe a successive breaking of the metal−metal bonds once the 3-fold degenerated $t_2$ orbital set becomes more than half-full at $x \geq 2$. The structure gradually changes from the $GaMo_4S_8$ type to the defect spinel type without filling of the 4*c* tetrahedral holes.

X-ray diffraction cannot distinguish Cr and V because of almost identical scattering powers. We are also unable to resolve

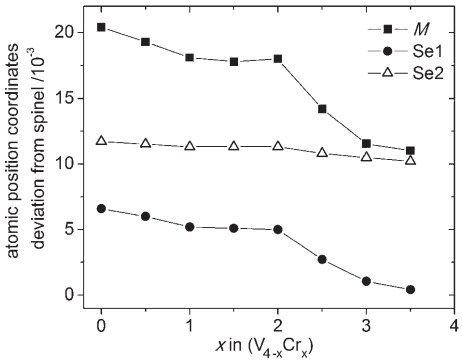


**Figure 5.** Deviation of coordinates from the ideal spinel structure type.

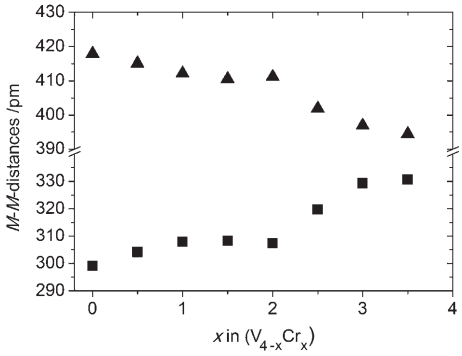


**Figure 6.** Intercluster (■) and intracluster (▲) $M-M$ distances. Error bars are smaller than the symbols.

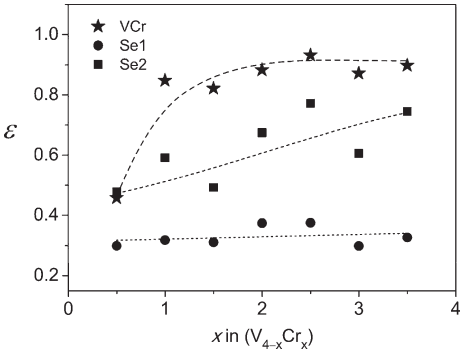


**Figure 7.** First eccentricities of the mean square displacement (msd) ellipsoids from single-crystal structure refinements. Dashed lines are guides to the eye.

differences in the V and Cr positions that are smaller than our experimental resolution of ~0.7 Å. Nevertheless, we have detected an increasing anisotropy of the thermal displacement parameters, especially when $0 \leq x \leq 2$. The latter affects the V/Cr and Se2 atoms that are connected to the $M_4$ cluster, but not the Se1 atoms of the $GaSe_4$ tetrahedra. The first eccentricities of the mean square displacement (msd) ellipsoids, defined as $\varepsilon = (1 - \mathrm{msd}_{min}/\mathrm{msd}_{max})^{1/2}$, are plotted versus the Cr concentration in Figure 7.

Even though these data are sensitive to errors, the trend is clearly visible. The elongation of the thermal ellipsoids along the body diagonal increases up to $x \sim 2$ and is saturated at higher Cr


dx.doi.org/10.1021/cm200776v |*Chem. Mater.* 2011, 23, 3014–3019

concentrations. This indicates slightly different coordinates of V and Cr at the (*x*,*x*,*x*) site. The directly bonded Se2 atoms are also affected, while the Se1 ellipsoides of the $GaSe_4$ tetrahedra remain almost spherical.

**Magnetism.** The temperature dependencies of the magnetic susceptibilities are shown in Figure 8, and the resultant magnetic parameters are listed in Table 1. The magnetic moment increases with the chromium concentration. Each Cr atom adds one electron to the 3-fold degenerated $t_2$ level of the tetrahedral cluster; thus, according to Hund's rule, the resulting magnetic moments should be compatible with $x + 1$ unpaired electrons per $M_4$ cluster. Figure 9 displays the experimental and anticipated magnetic moments expected by the cluster model (Figure 2) and by four nonbonded $M^{3.25+}$ ions. When $x \leq 2$, the experimental moments are in good agreement with the cluster model. When $x > 2$, the magnetic moment should decrease with additional Cr atoms, because the additional electrons should undergo spin pairing in the $t_2$ orbitals. However, in contrast to this, the experimental magnetic moments increase further with increasing Cr content nearly up to values expected from noninteracting $M^{3.25+}$ ions ($3M^{3+} + M^{4+}$). Obviously, the simple cluster model is not valid when $x > 2$. This is in line with the suddenly increasing $M-M$ distances measured via X-ray diffraction once $x \geq 2$. In this concentration range, neither the cluster model nor noninteracting ions reasonably describe the magnetic data, but if we assume that when $x > 2$ all V atoms are part of $V_2Cr_2$ clusters (maximal spin moment) and the additional Cr atoms are noninteracting, we obtain a much better congruence with the measured magnetic moments (dotted line in Figure 9).

Magnetization measurements at 2 K of selected samples are given in Figure 10. The sample with $x = 1$ is an example of a V-rich compound that shows almost ferromagnetic saturation as $GaV_4Se_8$. Nonetheless, the magnetic moments measured at 5 T in all samples are smaller than those expected from pure ferromagnetic ordering. The moment for $GaV_3CrSe_8$ is close to 1 $\mu_B$, while it should be close to 2 $\mu_B$ for two unpaired electrons per $M_4$ cluster. All samples for which $x \leq 2$ show the same ferromagnetic behavior but saturation moments that remain below the expected values. Perhaps magnetic ordering can occur only in domains with pure $V_4$ clusters and not in domains with mixed clusters. With increasing Cr content, the amounts of such domains decrease and so will the overall magnetic saturation moment. Zero-field cooled−field cooled (ZFC−FC) measurements of all those samples resulted in the Curie temperatures listed in Table 1. One example is shown in Figure 11.

Compounds for which $x > 2$ show a linear dependence of the magnetic moment on the magnetic field. Pronounced kinks in the susceptibility measurements indicate antiferromagnetic ordering. Néel temperatures were estimated from derivatives of the susceptibility measurements and are listed in Table 1.

**Electrical Resistivities.** Measurements of the temperature-dependent electrical resistivities show semiconducting behavior for all samples, as depicted in Figure 12. Activation energies ($E_a$) were estimated from Arrhenius plots (Table 1); the values roughly decrease from 0.27 eV at $x = 0.0$ to 0.05 eV at $x = 3.5$. This decrease in the size of the Mott−Hubbard gap may be attributed to the disbanding of the clusters, which releases additional mobile electrons. However, we note that the accuracy of the $E_a$ values is not better than ±0.1 eV

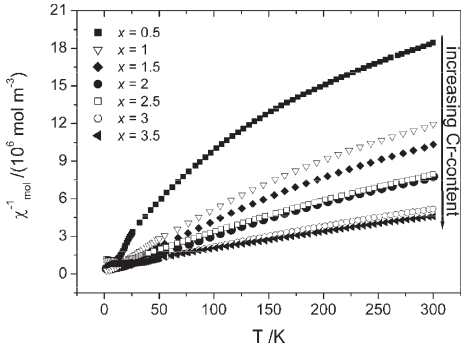


**Figure 8.** Inverse molar susceptibilities of $GaV_{4-x}Cr_xSe_8$.

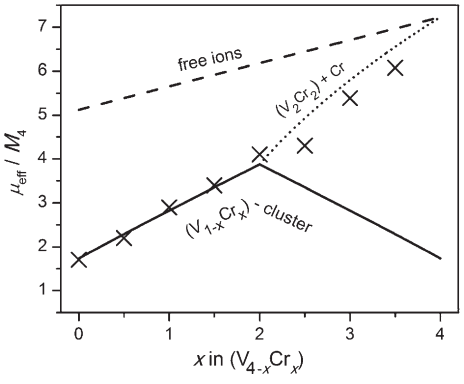


**Figure 9.** Effective magnetic moments per $M_4$ cluster. Errors are smaller than the symbols. The solid line shows theoretical values for the cluster model, the straight, dashed line values for noninteracting $M^{n+}$ ions, and the dotted line values for a model with noninteracting $Cr^{3.25+}$ ions and $V_2Cr_2$ clusters.

**Table 1. Magnetic Data and Activation Energies of $GaV_{4-x}Cr_xSe_8$**

| *x* | $\mu_{eff}$/4 *M* atoms (±0.1) | no. of unpaired electrons/ 4 *M* atoms (±0.1) | $\theta^a$ (K) | $T_C$ (K) | $T_N$ (K) | $E_a$ (eV) (±0.1) |
|---|---|---|---|---|---|---|
| 0 | 1.7 | 1 | 5(1) | 10 | – | 0.27 |
| 0.5 | 2.4 | 1.6 | 14(2) | 10 | – | 0.24 |
| 1 | 2.9 | 2.1 | 18(5) | 10 | – | 0.15 |
| 1.5 | 3.4 | 2.5 | 11(1) | 9 | – | 0.1 |
| 2 | 4.1 | 3.2 | 6(1) | 12 | – | 0.08 |
| 2.5 | 4.3 | 3.4 | −10(1) | – | 16 | 0.1 |
| 3 | 5.4 | 4.5 | −10(1) | – | 18 | 0.08 |
| 3.5 | 6.1 | 5.2 | −29(1) | – | 35 | 0.05 |

[a] Standard deviations of the last digit are given in parentheses.


dx.doi.org/10.1021/cm200776v |*Chem. Mater.* 2011, 23, 3014–3019

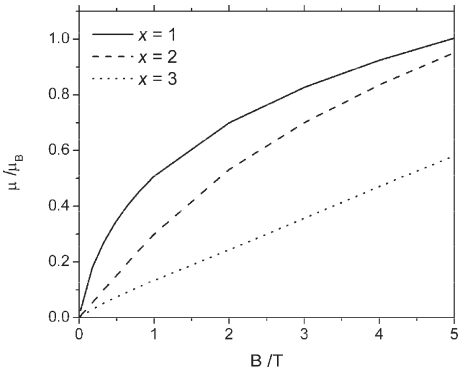


**Figure 10.** Magnetization isotherms of $GaV_3CrSe_8$ (—), $GaV_2Cr_2Se_8$ (---), and $GaVCr_3Se_8$ (· · ·) at 2 K.

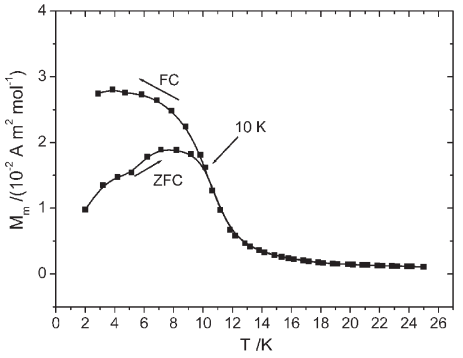


**Figure 11.** Zero-field cooled−field cooled measurements of $GaV_3CrSe_8$.

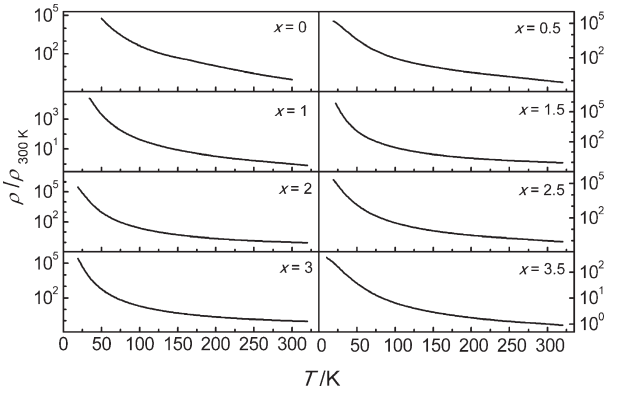


**Figure 12.** Normalized resistivities of $GaV_{4-x}Cr_xSe_8$.

**DFT Calculations.** To model theoretically the interplay between $M-M$ distances and magnetism, the positions of the $M$ atoms in $GaV_4Se_8$ and (hypothetical) $GaCr_4Se_8$ were varied in quantum chemical calculations. Energy differences are plotted in Figure 13. The minimum for $GaV_4Se_8$ occurs when $x \approx 0.601$, which means a state with $V_4$ clusters. $GaCr_4Se_8$ had two minima when the magnetic moment was optimized during the calculations, one at $x \approx 0.601$ with a small moment and the global one at $x \approx 0.617$ with a much larger moment. These values are in good agreement with the experimental values of $GaV_4Se_8$ and $GaV_{0.5}Cr_{3.5}Se_8$ obtained by single-crystal X-ray diffraction (see Figure 13). When the magnetic moment of $GaCr_4Se_8$ was fixed to one

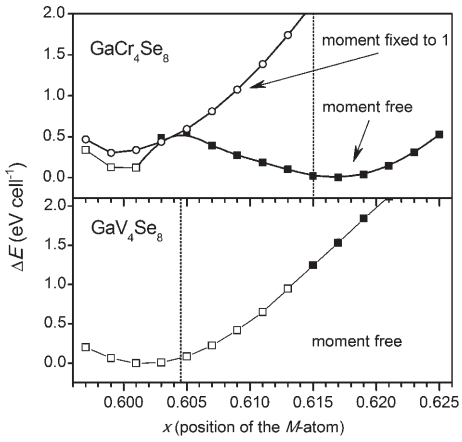


**Figure 13.** Relative energies vs the position of the $M$ atoms in hypothetical $GaCr_4Se_8$ and $GaV_4Se_8$. Filled data points represent magnetic moments greater than one unpaired electron. Vertical dotted lines mark the experimental positions of $M$ atoms in $GaV_4Se_8$ and $GaV_{0.5}Cr_{3.5}Se_8$ from X-ray diffraction.

unpaired electron per $Cr_4$, the lowest energy is also around 0.600, indicating $Cr_4$ clusters. This clearly shows how the clusters existing in $GaV_4Se_8$ disband in $GaCr_4Se_8$. The resulting numbers of unpaired electrons per four $M$ atoms are 1 for $GaV_4Se_8$ and 5.8 for $GaCr_4Se_8$, which again correspond very well to experiment, where we find 1 unpaired electron for $GaV_4Se_8$ where the other electrons are paired in metal−metal bonds and ≈5 for $GaV_{0.5}Cr_{3.5}Se_8$.

## DISCUSSION

Magnetic measurements and X-ray diffraction data are consistent with $M-M$ bonds in $GaV_{4-x}Cr_xSe_8$ for $x < 2$. Most electrons of the metals are paired in these bonds of the tetrahedral $M_4$ clusters. In the Cr-rich region ($x > 2$), these clusters disintegrate or at least no clusters with a Cr content higher than a 1:1 V:Cr ratio are formed. The resulting structure is a defect spinel-type structure in which the average distances between $M$ atoms are too large to be considered bonds. This behavior is similar to that of $Ga_xV_{4-y}Cr_yS_8$ reported previously,[22] but in the latter case, additional Ga atoms were introduced at the 4*c* Wyckoff position in the Cr-rich region ($y > 2$), which naturally leads to a spinel-like structure in α-$Ga_{1.33}Cr_4S_8$[29] with only $Cr^{3+}$ ions. The additional Ga atoms formally reduce chromium to $Cr^{3+}$, which is known to be the highest stable oxidation number for chromium in sulfides. In the selenium compounds presented in this paper, the clusters also dissolve, but without additional atoms in the structure; thus, this is an entirely electronic effect.

The magnetic properties of $GaV_{4-x}Cr_xSe_8$ can be explained as follows. When $x < 2$, the cluster model fits the experimental data very well, but when $x > 2$, it does not; crystallographic data suggest separated $M^{3.25+}$ ions. However, the experimental magnetic moments remain lower than the expected values, as indicated by the dashed line in Figure 9. We suggest that clusters with more than nine electrons (half-full $t_2$ set) are unstable and thus not formed. Therefore, we expect $Cr_2V_2$ clusters and nonbonded Cr ions in Cr-rich samples ($x > 2$). The resulting magnetic moment would be lower than the one from purely noninteracting $M^{3.25+}$ ions (one $Cr_2V_2$ cluster carries only 3 spins per cluster and one $M^{3.25+}$ ion an average 2.75 spins per atom). Theoretical values from this model are presented with the dotted line in Figure 9, which is close to the experimental data.


dx.doi.org/10.1021/cm200776v |*Chem. Mater.* 2011, 23, 3014–3019

Nonetheless, X-ray diffraction data provide no direct proof for this model. Because of almost identical X-ray scattering powers of Cr and V and the very small changes in the positions that distinguish between cluster formation and separated ions, we were able to refine only one position for Cr/V, but the increasing anisotropy of the thermal displacement parameters at higher Cr concentrations clearly indicates slightly different positions of V and Cr. We suggest that Cr prefers positions with increasingly longer Cr−*M* bonds at higher Cr concentrations, in good agreement with our model. There is an additional supporting argument. The calculated position of Cr in hypothetical $GaCr_4Se_8$ is 16*e* (*x*,*x*,*x*), where $x = 0.617$. This should be the expected position of Cr in Cr-rich compounds, but the measured positions for all Cr-rich samples show smaller values between 0.607 ($GaV_2Cr_2Se_8$) and 0.614 ($GaV_{0.5}Cr_{3.5}Se_8$). This is indicative of averaging between a cluster compound and a spinel-like compound in the diffraction experiment.

## CONCLUSION

The solid solution $GaV_{4-x}Cr_xSe_8$ ($x = 0-4$) is an unprecedented example of the interplay between metal−metal bond formation in clusters and the formation of magnetic moments. We have shown how the increased filling of the cluster molecular orbitals destabilizes the bonds as soon as the degenerated $t_2$ orbitals become more than half-full. Metal−metal bonds vanish, and the electrons that previously formed these bonds become unpaired and strongly increase the magnetism of the system. Thus, the material switches between a metal−metal bonded weak magnetic state and a nonbonded strong magnetic state. This is an entirely electronic effect in contrast to that of the sulfide material reported earlier.

## ASSOCIATED CONTENT

**Supporting Information.** Crystallographic data (CIF). This material is available free of charge via the Internet at http://pubs.acs.org.

## AUTHOR INFORMATION

**Corresponding Author**
*E-mail: dirk.johrendt@cup.uni-muenchen.de.

## ACKNOWLEDGMENT

This work was financially supported by Deutsche Forschungsgemeinschaft (DFG) Project Jo257/4-2.

## REFERENCES

(1) Perrin, C.; Chevrel, R.; Sergent, M. *C. R. Seances Acad. Sci., Ser. C* **1975**, *280* (14), 949–951.
(2) Pocha, R.; Johrendt, D.; Pöttgen, R. *Chem. Mater.* **2000**, *12* (10), 2882–2887.
(3) Pocha, R.; Johrendt, D.; Ni, B.; Abd-Elmeguid, M. M. *J. Am. Chem. Soc.* **2005**, *127* (24), 8732–8740.
(4) Ben Yaich, H.; Jegaden, J. C.; Potel, M.; Sergent, M.; Rastogi, A. K.; Tournier, R. *J. Less-Common Met.* **1984**, *102* (1), 9–22.
(5) Barz, H. *Mater. Res. Bull.* **1973**, *8* (8), 983–988.
(6) Vaju, C.; Martial, J.; Janod, E.; Corraze, B.; Fernandez, V.; Cario, L. *Chem. Mater.* **2008**, *20* (6), 2382–2387.
(7) Rastogi, A. K.; Berton, A.; Chaussy, J.; Tournier, R.; Potel, M.; Chevrel, R.; Sergent, M. *J. Low Temp. Phys.* **1983**, *52* (5−6), 539–557.
(8) Francois, M.; Lengauer, W.; Yvon, K.; Ben Yaich-Aerrache, H.; Gougeon, P.; Potel, M.; Sergent, M. *Z. Kristallogr.* **1991**, *196* (1−4), 111–120.
(9) Müller, H.; Kockelmann, W.; Johrendt, D. *Chem. Mater.* **2006**, *18* (8), 2174–2180.
(10) Rastogi, A. K.; Wohlfarth, E. P. *Phys. Status Solidi B* **1987**, *142* (2), 569–573.
(11) Abd-Elmeguid, M. M.; Ni, B.; Khomskii, D. I.; Pocha, R.; Johrendt, D.; Wang, X.; Syassen, K. *Phys. Rev. Lett.* **2004**, *93* (12), 126403/1–126403/4.
(12) Dorolti, E.; Cario, L.; Corraze, B.; Janod, E.; Vaju, C.; Koo, H. J.; Kan, E.; Whangbo, M. H. *J. Am. Chem. Soc.* **2010**, *132* (16), 5704–5710.
(13) Vaju, C.; Cario, L.; Corraze, B.; Janod, E.; Dubost, V.; Cren, T.; Roditchev, D.; Braithwaite, D.; Chauvet, O. *Adv. Mater.* **2008**, *20* (14), 2760.
(14) Cario, L.; Vaju, C.; Corraze, B.; Guiot, V.; Janod, E. *Adv. Mater.* **2010**, *22* (45), 5193.
(15) Rastogi, A. K.; Niazi, A. *Phys. B (Amsterdam, Neth.)* **1996**, *223−224* (1−4), 588–590.
(16) Sahoo, Y.; Rastogi, A. K. *Phys. B (Amsterdam, Neth.)* **1995**, *215* (2−3), 233–242.
(17) Sahoo, Y.; Rastogi, A. K. *J. Phys.: Condens. Matter* **1993**, *5* (32), 5953–5962.
(18) Shanthi, N.; Sarma, D. D. *J. Solid State Chem.* **1999**, *148* (1), 143–149.
(19) Nakamura, H.; Chudo, H.; Shiga, M. *J. Phys.: Condens. Matter* **2005**, *17* (38), 6015–6024.
(20) Johrendt, D. *Z. Anorg. Allg. Chem.* **1998**, *624* (6), 952–958.
(21) Le Beuze, A.; Loirat, H.; Zerrouki, M. C.; Lissillour, R. *J. Solid State Chem.* **1995**, *120* (1), 80–89.
(22) Bichler, D.; Johrendt, D. *Chem. Mater.* **2007**, *19*, 4316–4321.
(23) X-RED32. *X-RED data reduction*, version 1.26; Stoe & Cie GmbH: Darmstadt, Germany, 2004.
(24) Sheldrick, G. M. *Acta Crystallogr.* **2008**, *A64* (1), 112–122.
(25) *Low Level Measurements, Precision DC Current, Voltage and Resistance Measurements*, 5th ed.; Keithley Instruments, Inc.: Cleveland, OH, 1998.
(26) Lueken, H. *Magnetochemie*; Teubner: Stuttgart, Germany, 1999.
(27) Blaha, P.; Schwarz, K.; Madsen, G. K. H.; Kvasnicka, D.; Luitz, J. *WIEN2k: An Augmented Plane Wave + Local Orbitals Program for Calculating Crystal Properties*, version 6; Vienna University of Technology: Vienna, 2001.
(28) Perdew, J. P.; Burke, K.; Ernzerhof, M. *Phys. Rev. Lett.* **1996**, *77* (18), 3865–3868.
(29) Ben Yaich, H.; Jegaden, J. C.; Potel, M.; Sergent, M.; Huguet, P.; Alquier, G. *Mater. Res. Bull.* **1983**, *18* (7), 853–860.